State of the art timing in TOF-PET detectors with LuAG, GAGG and L(Y)SO scintillators of various sizes coupled to FBK-SiPMs

2016 JINST 11 P08008

(http://iopscience.iop.org/1748-0221/11/08/P08008)

Published by IOP Publishing for Sissa Medialab

Received: *May 20, 2016*
Revised: *July 29, 2016*
Accepted: *July 30, 2016*
Published: *August 8, 2016*

State of the art timing in TOF-PET detectors with LuAG, GAGG and L(Y)SO scintillators of various sizes coupled to FBK-SiPMs

S. Gundacker,[a,1] **F. Acerbi,**[b] **E. Auffray,**[a] **A. Ferri,**[b] **A. Gola,**[b] **M.V. Nemallapudi,**[a] **G. Paternoster,**[b] **C. Piemonte**[b] **and P. Lecoq**[a]

[a] *European Organization for Nuclear Research (CERN), 1211 Geneva 23, Switzerland*
[b] *Fondazione Bruno Kessler, via Sommarive 18, Trento, Italy*

E-mail: stefan.gundacker@cern.ch

Abstract: Time of flight (TOF) in positron emission tomography (PET) has experienced a revival of interest after its first introduction in the eighties. This is due to a significant progress in solid state photodetectors (SiPMs) and newly developed scintillators (LSO and its derivatives). Latest developments at Fondazione Bruno Kessler (FBK) lead to the NUV-HD SiPM with a very high photon detection efficiency of around 55%. Despite the large area of $4 \times 4\,mm^2$ it achieves a good single photon time resolution (SPTR) of 180±5ps FWHM. Coincidence time resolution (CTR) measurements using LSO:Ce codoped with Ca scintillators yield best values of 73±2ps FWHM for $2 \times 2 \times 3\,mm^3$ and 117±3ps for $2 \times 2 \times 20\,mm^3$ crystal sizes. Increasing the crystal cross-section from $2 \times 2\,mm^2$ to $3 \times 3\,mm^2$ a non negligible CTR deterioration of approximately 7ps FWHM is observed. Measurements with LSO:Ce codoped Ca and LYSO:Ce scintillators with various cross-sections ($1 \times 1\,mm^2$ - $4 \times 4\,mm^2$) and lengths (3mm - 30mm) will be a basis for discussing on how the crystal geometry affects timing in TOF-PET. Special attention is given to SiPM parameters, e.g. SPTR and optical crosstalk, and their measured dependency on the crystal cross-section. Additionally, CTR measurements with LuAG:Ce, LuAG:Pr and GGAG:Ce samples are presented and the results are interpreted in terms of their scintillation properties, e.g. rise time, decay time, light yield and emission spectra.

Keywords: Gamma camera, SPECT, PET PET/CT, coronary CT angiography (CTA); Photon detectors for UV, visible and IR photons (solid-state) (PIN diodes, APDs, Si-PMTs, G-APDs, CCDs, EBCCDs, EMCCDs etc); Scintillators, scintillation and light emission processes (solid, gas and liquid scintillators); Timing detectors

[1] Corresponding author.

doi:10.1088/1748-0221/11/08/P08008

Contents

2016 JINST 11 P08008

1 Introduction

Scintillator based detectors for time-of-flight positron emission tomography (TOF-PET) are able to achieve very good timing approaching a coincidence time resolution (CTR) of 100ps FWHM, as shown in several publications [1, 2]. This is due to a significant progress in solid state photodetectors, e.g the silicon photomultiplier (SiPM), which facilitates excellent timing properties and a high photon detection efficiency (PDE). Additionally to the advances in SiPMs, scintillator materials like Cerium-doped Lutetium Oxyorthosilicate (LSO:Ce) and its derivatives show a high light yield, fast decay and rise times and a very high effective atomic number. The progress made allows for very fast timing, keeping a high 511keV absorption coefficient with a high photoelectric fraction.

NUV-HD SiPMs are the latest development of FBK (Fondazione Bruno Kessler), representing the state of the art in SiPM photodetector technology regarding photon detection efficiency (PDE) and single photon time resolution (SPTR). These photodetectors, if coupled to LYSO:Ce scintillators with $3\times3\times5$ mm^3 dimensions are able to achieve ~100ps FWHM, as was recently published in [3]. In this paper it will be shown that these good results can almost be retained (within 20%) if using

state of the art LSO:Ce codoped Ca crystals of 20mm length, particularly interesting for applications in TOF-PET.

In whole body PET the number of electronic channels is an important issue and should be reduced in order to keep complexity and cost low. Hence, an increase in the SiPM and crystal cross-section is anticipated. Measurements with various crystal cross-sections ($1 \times 1\,mm^2$ - $4 \times 4\,mm^2$) will be presented and interpreted within further complementary measurements and Monte Carlo simulations.

Furthermore, we present latest CTR values measured for different crystal compositions, i.e. LuAG and GAGG doped with Cerium. The effect of codoping with either Magnesium or Calcium is discussed as well [4–6]. Codoped scintillators are particularly interesting because of their faster scintillation rise times and decay times leading to improved timing [7]. Additionally, prompt photons have been seen and clearly separated from the scintillation signal in some compositions, e.g. LuAG:Pr [7]. These prompt photons are produced most likely by the Cherenkov effect, although some other contributions, for instance from hot-intraband-luminescence are not excluded [8]. The Cherenkov effect has already been studied in several publications and its potential influence to the CTR discussed [7, 9, 10]. However, until now there was no clear evaluation on how the CTR is affected by these prompt photons. We will show that prompt photons in LuAG:Pr and LuAG:Ce are important to estimate the CTR correctly. Additional comprehensive Monte Carlo simulations of the CTR will be evaluated with experimental data, using the measured prompt photon yield, scintillation light yield, rise- and decay-times.

2 Materials and methods

2.1 FBK NUV-HD SiPM

The NUV-HD (near ultraviolet - high density) SiPM is a new development done at FBK which implements a new microcell border structure similar to the technology utilized for the RGB-HD devices [3]. This allows to increase the fill factor of the device, despite a relatively small single avalanche photodiode (SPAD) size of $25 \times 25\,\mu m^2$, and hence increases the photon detection efficiency (PDE). The smaller cell size additionally allows for a higher operational bias overvoltage and thus boosts the PDE further. The higher overvoltage achievable is mainly explained by a decreased gain of smaller SPADs and thus a decreased optical crosstalk probability [11]. On the left hand side in figure 1 it can be seen that for the NUV-HD SiPM, with coupled crystal, the maximum applicable operational overvoltage is 13V before the bias current increases drastically. In our former publication [12] we showed that this exact behavior happens already at ~6V for the NUV type SiPM. The right hand side of figure 1 shows the PDE of the NUV and NUV-HD SiPM plotted versus the wavelength. It can be seen that the NUV SiPM achieves a maximum PDE of 40% whilst the NUV-HD SiPM can reach values as high as 55%. PDE values were measured at 6V overvoltage and 13V overvoltage for the NUV and NUV-HD SiPM, respectively - representing the maximum possible operational overvoltages.

2.2 Coincidence time resolution measurements

The coincidence time resolution (CTR) was measured with our standard setup as described in [2] and shown in figure 2. For these measurements the scintillators were wrapped in Teflon, at least

2016 JINST 11 P08008

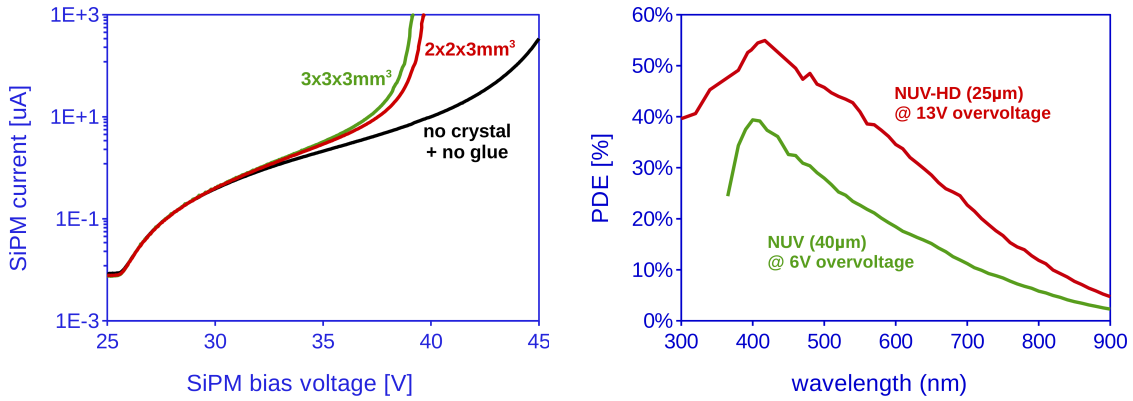

(a) (b)

Figure 1. (a) NUV-HD bias current as a function of bias voltage applied. Breakdown voltage is 25.5V and the maximum applicable voltage for operation is ~ 38.5V. (b) Photon detection efficiency of the NUV and NUV-HD SiPM at maximum operational overvoltages.

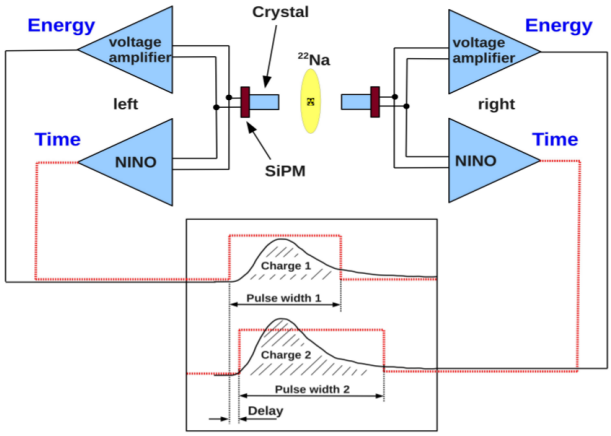

Data acquisition:
LeCroy Oscilloscope DDA 735Zi with
3.5GHz Bandwith and 40Gs/s

Figure 2. Coincidence time resolution setup as described in [2].

five layers, and optically coupled to the SiPM (NUV-HD) with Meltmount (n = 1.68). The crystals were polished on all six faces, if not otherwise stated.

The signals generated by the SiPM were readout by NINO [13], a low noise leading edge threshold discriminator amplifier, which delivered the time information and a voltage amplifier for energy discrimination. The splitting of the energy and timing signal is necessary in order to be able to optimize both channels independently for best performance, i.e. for energy and time resolution. The reason is that typically the leading edge discrimination is performed at very low threshold voltages in the order of the single cell signal amplitude of the SiPM (one SPAD signal), which needs amplification. On the other hand the energy signal amplitude is several orders of magnitude larger, calling for a different readout strategy with much lower amplification, sometimes even attenuation. The timing and energy signals were digitized and stored on disk by a fast

2016 JINST 11 P08008

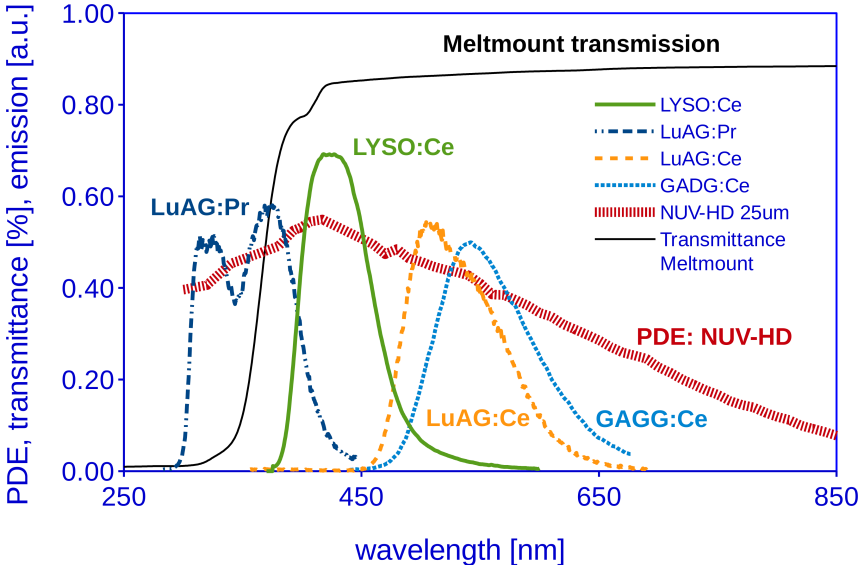

Figure 3. Emission spectra of the studied scintillating materials plotted alongside the PDE of the NUV-HD SiPM and the transmittance of the used Meltmount glue (n = 1.68).

oscilloscope (LeCroy DDA 735Zi with 3.5GHz bandwidth and 40Gs/s). In the offline data analysis we only selected events within the photopeak (-1.5σ to $+2\sigma$ around the centroid μ), representing the whole energy of 511keV deposited in the crystal. We want to mention that studies on the photopeak-selection have shown that the width of valid events plays a minor (almost negligible) role in the obtained CTR. This is mainly explained by a sufficient energy resolution which allows for a clear cut between Compton and photoelectric events [14]. For the selected events within the photopeak we plotted the time delays in a histogram and applied a Gaussian fit on the data yielding the coincidence time resolution in full width at half maximum (FWHM), as described in [2]. The temperature was stabilized at 15°C for all ensuing measurements.

2.3 Scintillator materials

We tested different scintillator materials activated with Cerium, i.e. LSO:Ce and LSO:Ce codoped with 0.2%Ca or 0.4%Ca from the producer Agile, LYSO:Ce from the producer CPI, LuAG:Ce and LuAG:Ce codoped Ca produced in Ashtarak (Ashot Petrosyan) [4], GAGG:Ce and GAGG:Ce codoped Mg produced in Prague (Martin Nikl) [5]. Additionally we measured LuAG activated with Praseodymium (Pr) produced in Ashtarak [4]. The emission spectra of the tested materials can be seen in figure 3. The measured emission of LuAG:Ce codoped Ca or GAGG:Ce codoped Mg have an identical spectra with respect to LuAG:Ce or GAGG:Ce, and hence are not depicted in figure 3. The same applies for LYSO:Ce and LSO:Ce codoped Ca.

In table 1 measurements of the scintillation characteristics of the tested materials are summarized, i.e. rise time, decay times, relative light yield and scintillation light detection probability (PDE·LTE). The detection probability (PDE·LTE) describes the PDE weighted with the emission spectra of the scintillator, taking into account the Meltmount transmission, multiplied with the light transfer efficiency (LTE) of the crystal. In our following Monte Carlo simulations we used these values and took an intrinsic light yield value of 40kph/MeV for LYSO:Ce [15].

2016 JINST 11 P08008

Table 1. Measured scintillation properties of the tested materials. Values are partly taken from our previous measurements published in [5, 7]. Light output (LO) measurements were performed with $2 \times 2 \times 10\,\mathrm{mm}^3$ crystals (and $2{\times}2{\times}8\,\mathrm{mm}^3$ for LuAG) wrapped in Teflon and optically coupled with Rhodorsil 47V ($n = 1.42$). A Hamamatsu PMT R2059 was used for the relative light output measurements, normalized to LYSO:Ce. The relative error of the LY and decay time measurements is in the order of ±5%, whereas the statistical uncertainty of the rise time is stated in the table. Note: the light output value for LuAG:Pr underlies a higher uncertainty due to its emission in the UV together with uncertainties in the transmittance of the used Rhodorsil 47V grease.

sample	τ_r [ps]	τ_{d1} (R_1) [ns] ([%])	τ_{d2} (R_2) [ns] ([%])	τ_{d3} (R_3) [ns] ([%])	reference	rel. LO [%]	PDE · LTE [%]
LSO:Ce:0.4%Ca	21±20	8 (6)	33 (94)	—	[7]	80	26
LSO:Ce:0.2%Ca	9±9	10 (5)	35 (95)	—	(new)	98	26
LYSO:Ce	68±20	21 (12)	44 (88)	-	(new)	100	26
GAGG:Ce	1780±140	101 (65)	319 (35)	—	[5]	170	21
GAGG:Ce:Mg	54±27	51 (53)	196 (47)	—	[5]	118	21
LuAG:Pr	251±60	22 (52)	787 (48)	—	[7]	~54	11
LuAG:Ce	535±100	70 (44)	1063 (56)	—	[7]	58	23
LuAG:Ce:Ca	158±30	20 (12)	60 (62)	822 (26)	[7]	61	23

As can be seen in figure 3 the chosen Meltmount glue with a refractive index of $n = 1.68$ has a cut-off around 400nm which unfortunately is unfavorable for LuAG:Pr and halves the detected scintillation light as compared to LuAG:Ce. The light transfer efficiency, defined as the ratio of scintillation light reaching the photodetector and the total amount of light produced, was estimated by Monte Carlo simulations [2, 12] to be ~61% for LYSO:Ce scintillators with $2 \times 2 \times 10\,\mathrm{mm}^3$ size coupled to the FBK NUV-HD SiPM with Meltmount ($n = 1.68$). This value does not take into account the transmittance of the Meltmount glue, which is included in the effective PDE (column PDE·LTE in table 1). Similar LTE values were taken for LuAG and GAGG crystals. For LuAG crystals this is justified, because of the almost similar refractive index. In fact other influences, like small differences in diffusivity, e.g. surface or edge polishing, tendentiously can have a larger influence on the light transfer efficiency [16]. For GAGG crystals the exact determination of the LTE value is still subject to investigation, as the index of refraction, magnitude of bulk absorption and amount of re-absorption still need further evaluation. However, for the following CTR simulations this uncertainty in LTE is accounted for in the relative LO measurements, as shown in column 7 of table 1.

On the left hand side of figure 4 we show transmission measurements of $2 \times 2 \times 10\,\mathrm{mm}^3$ sized LYSO:Ce, LSO:Ce codoped 0.2%Ca and LSO:Ce codoped 0.4%Ca crystals. Whereas on the right hand side of figure 4 similar measurements for $2 \times 2 \times 20\,\mathrm{mm}^3$ crystals are shown. We observe that with increasing crystal length the transmission becomes significantly worse in LSO:Ce codoped 0.4%Ca crystals as compared to LYSO:Ce and LSO:Ce codoped 0.2%Ca. However, it should be mentioned that the Agile LSO:Ce:0.4%Ca samples are from an older production batch (2011) as compared to the Agile LSO:Ce:0.2%Ca and LYSO:Ce crystals (2016). Therefore, it might be possible that the observed increase in re-absorption is a feature of our particular samples and not generally valid.

2016 JINST 11 P08008

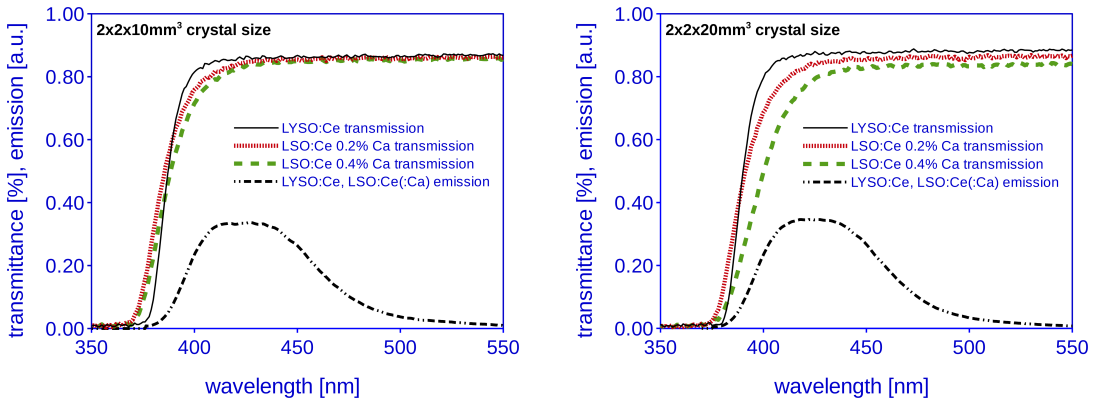

(a) (b)

Figure 4. Transmission measured with LYSO:Ce, LSO:Ce codoped with 0.2%Ca and LSO:Ce codoped with 0.4%Ca shown alongside their emission spectra. (a) For 10mm crystal lengths only marginal differences in the transmission can be seen. With slightly worse transmission for the Ca codoped samples. (b) For 20mm long crystals a worse transmission is observed for the LSO:Ce:0.4%Ca samples as compared to LYSO:Ce and LSO:Ce:0.2%Ca.

3 Results

3.1 Time resolution with LSO:Ce codoped with 0,4%Ca and LYSO:Ce

We measured the coincidence time resolution with LSO:Ce codoped with 0.4%Ca crystals from the producer Agile and LYSO:Ce from the producer CPI with the measurement details already discussed in section 2.2. In figure 5 the CTR versus the bias overvoltage and NINO threshold voltage is shown for $2 \times 2 \times 3\,\mathrm{mm}^3$ LSO:Ce:0.4%Ca crystals coupled to the NUV-HD SiPM. A best CTR value of 73±2ps FWHM is achieved at an overvoltage of 12.5V and a NINO threshold voltage of ~120mV, which corresponds to 1 SiPM single cell signal amplitude (SPAD signal amplitude). However, it should be noted that the number of photoelectrons contributing to the leading edge time estimation is much higher and more in the order of several photoelectrons [2, 17]. A clear improvement in CTR with bias overvoltage is observed, which is explained by an increase in PDE plus a decrease in SPTR value for higher overvoltages. On the right hand side of figure 5 it can be seen that for low threshold values electronic noise worsens the time resolution and that for higher threshold values photonstatistics leads to worse CTR, hence, resulting in the optimum NINO threshold voltage at around 120mV [1, 2, 17]. The CTR improvement as compared to our former publication with the NUV SiPM (85±4ps FWHM with $2 \times 2 \times 3\,\mathrm{mm}^3$ LSO:Ce codoped 0.4%Ca) [12] can be entirely explained by the higher PDE the NUV-HD SiPM achieves, as was discussed in section 2.1.

We additionally performed measurements with various lengths of the codoped 0.4%Ca LSO:Ce crystals, ranging from 3mm to 20mm, the results of which are shown in figure 6. A deterioration in CTR for longer crystals is observed, due to an increased photon travel spread (PTS) and decreased light transfer efficiency (LTE) [18]. CTR values for $2 \times 2 \times 20\,\mathrm{mm}^3$ crystal sizes are measured to reach values as low as 122±3ps FWHM.

In addition to LSO:Ce:0,4%Ca we used standard LYSO:Ce crystals from the producer CPI and compared the best CTR values achievable, as can be seen on the left hand side of figure 7. For shorter crystals of $2 \times 2 \times 3\,\mathrm{mm}^3$ size the best CTR achieved for LYSO:Ce is 87±3ps FWHM,

2016 JINST 11 P08008

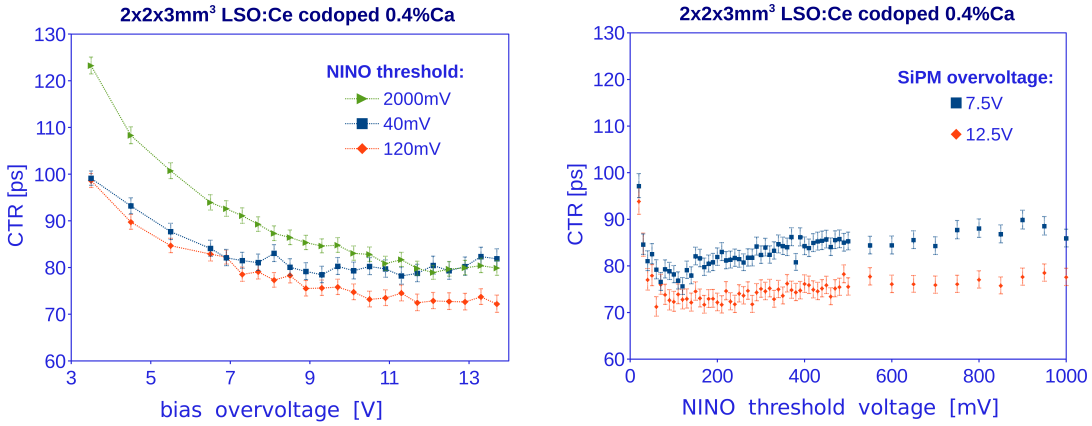

(a) (b)

Figure 5. CTR measurements with the NUV-HD and $2\times2\times3$ mm^3 LSO:Ce codoped 0.4%Ca crystals results in a best value of 73±2ps FWHM. (a) CTR as a function of SiPM bias overvoltage (breakdown voltage is 25.5V) and (b) CTR as a function of NINO leading edge threshold.

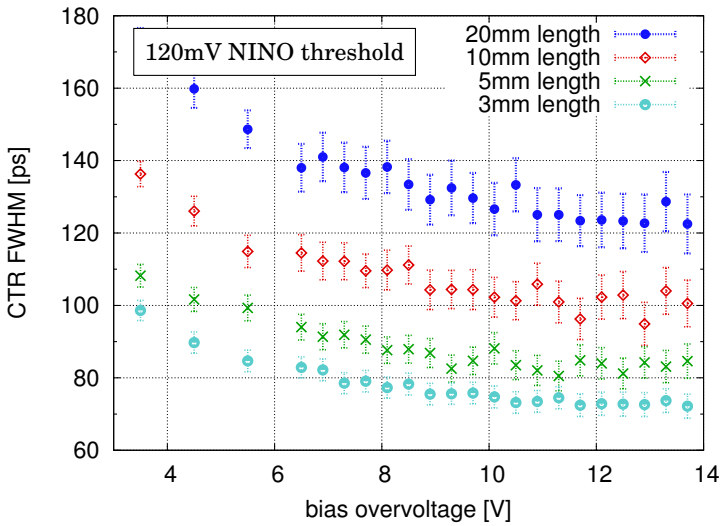

Figure 6. CTR measured with LSO:Ce codoped 0.4%Ca as a function of NUV-HD bias overvoltage for various crystal lengths. Short crystals of $2\times2\times3$ mm^3 achieve a CTR of 73±2ps FWHM, which deteriorates to 122±3ps FWHM for $2\times2\times20$ mm^3 crystals. Breakdown voltage is 25.5V.

compared to 73±2ps FWHM for LSO:Ce:0,4%Ca. The worse time resolution for LYSO:Ce can be explained by a longer scintillation decay time and a larger scintillation rise time, which are not compensated by the higher light output observed for LYSO:Ce (see table 1). However, if the crystal length is increased up to 20mm, we observe that LYSO:Ce gives almost the same performance of 130±3ps FWHM as compared to 122±3ps FWHM for LSO:Ce:0.4%Ca. This we could explain by a lower light absorption observed in LYSO:Ce than in LSO:Ce:0.4%Ca, to be seen on the right hand side of figure 7 and in figure 4. Increasing the LYSO:Ce crystal length even further, to 30mm, we obtain a CTR of 142±3ps FWHM.

2016 JINST 11 P08008

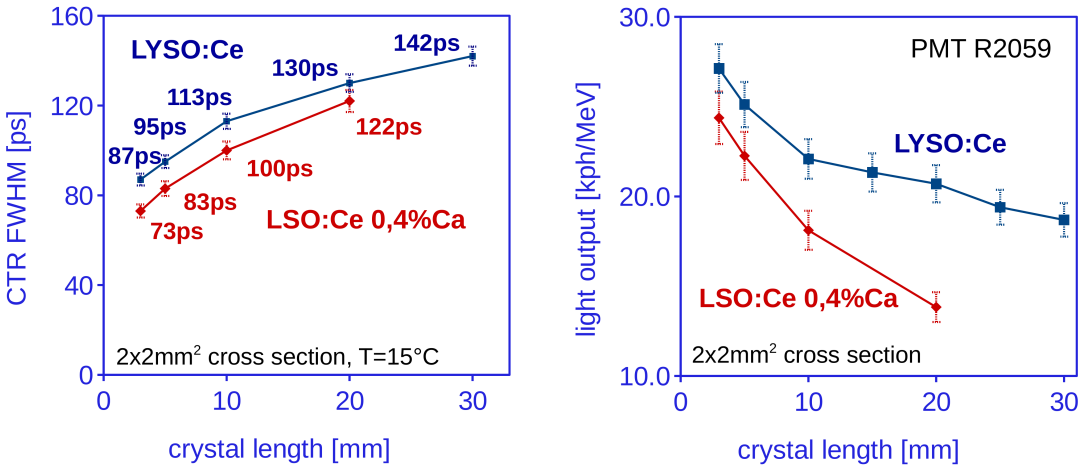

(a) (b)

Figure 7. (a) Investigating the CTR versus the crystal length shows that LYSO:Ce crystals perform almost similar to LSO:Ce:0.4%Ca for 20mm long crystals. (b) Measured light output versus the crystal length for LSO:Ce:0.4%Ca and LYSO:Ce reveals a lower light absorption for LYSO:Ce.

3.2 Limitations of the electronics and acquisition system

In order to test the limitations of the electronics (NINO) and acquisition system (oscilloscope) we tested our measurement setup by splitting one SiPM signal (with coupled $2 \times 2 \times 3\,\mathrm{mm}^3$ LSO:Ce codoped with 0.4%Ca crystal) and feeding it into two NINO chips. This gives the "intrinsic CTR", which represents the electronic noise influence on the leading edge discrimination with the correct signal generated from the SIPM+crystal plus the independent time jitter of the oscilloscope. In figure 8 the outcome of this measurement is shown, where threshold values are corrected for the slightly lower single cell amplitude due to the lower input impedance in this setup. The CTR "intrinsic" value decreases with increasing leading edge NINO threshold voltage and saturates at a value of 12ps FWHM. The saturation at 12ps is defined by the noise floor of NINO plus the oscilloscope and the dV/dt of the NINO output pulse recorded. The rise in CTR for lower threshold voltages is explained by the shape of the NINO input signal being a sum of single cell pulses and its dV/dt together with the NINO electronic noise and bandwidth filtering. In full generality it can be fitted with $532/(V_{\mathrm{Threshold}})^{0.79}$ for 12.5V overvoltage, as expressed by the green dotted line in figure 8. As already mentioned, this term represents the ratio of the electronic noise in the first stage of NINO divided by the dV/dt of the signal in this stage, i.e. $u_{\mathrm{noise}}/(dV/dt) = 532/(V_{\mathrm{Threshold}})^{0.79}$ for 12.5V. Supposing a noise level of $u_{\mathrm{noise}} = 0.01mV$ and a NINO threshold setting of $V_{\mathrm{Threshold}} = 100mV$ we would obtain an input stage slew rate of $dV/dt = 0.7mV/ns$ for the SiPM signal with multiple photoelectrons piled-up already. However, it should be mentioned that the slew rate is rather complex to estimate and depends not only on the electronics but as well on the scintillator photonemission and SiPM properties. Nonetheless, figure 8 shows one important conclusion; if very low leading edge thresholds are needed, e.g. for the detection of prompt photons like Cherenkov or in the case of low SPTR values, electronic noise can potentially limit the best achievable time resolution [7]. In these circumstances a digital approach might be viable [7, 17].

2016 JINST 11 P08008

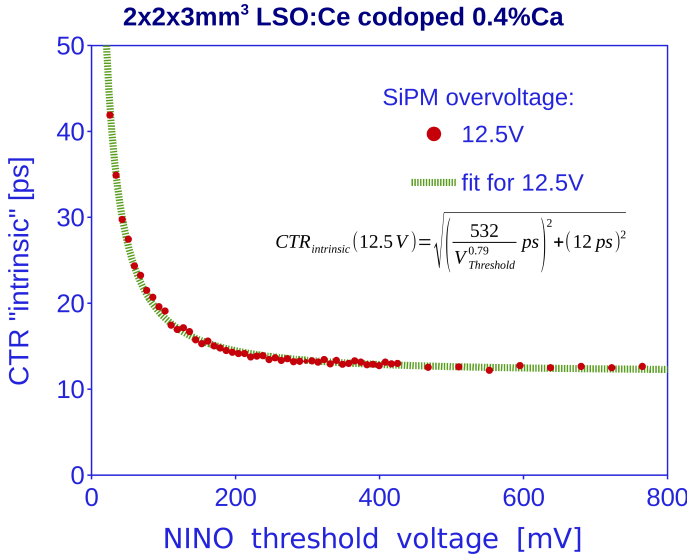

Figure 8. "Intrinsic" CTR of the electronics plus acquisition system. A $2 \times 2 \times 3\,\mathrm{mm}^3$ LSO:Ce:0.4%Ca crystal was coupled to a NUV-HD SiPM. The SiPM signal was split and fed into two NINO chips, measuring the delay times as in a standard CTR setup. This plot represents the lowest CTR FWHM achievable with the current electronics and data acquisition system.

3.3 Crystal cross-section influence on the time resolution

One possible way to reduce the number of electronic channels in a whole body TOF-PET machine is to increase the crystal cross-section, typically up to $4 \times 4\,\mathrm{mm}^2$ comparable to the resolution of commercially produced systems, e.g. [19]. In figures 9 and 10 we investigated how the time resolution is changing with increasing crystal cross-section, from $1 \times 1\,\mathrm{mm}^2$ up to $4 \times 4\,\mathrm{mm}^2$. All measurements shown are done with NUV-HD SiPMs from FBK which have a device area of $4 \times 4\,\mathrm{mm}^2$. As already discussed in section 2.2 the crystals were wrapped in Teflon (at least 5 layers) and coupled to the SiPM with Meltmount ($n = 1.68$). All six surfaces of the scintillators were polished.

We observe that an increase of crystal cross-section from $2 \times 2\,\mathrm{mm}^2$ to $3 \times 3\,\mathrm{mm}^2$ leads to an average CTR deterioration of ~7ps FWHM, consistent for 3mm and 20mm long crystals (as can be seen on the left hand side of figures 9 and 10). Coupling crystals with $4 \times 4\,\mathrm{mm}^2$ cross-section leads to an even higher CTR deterioration. However, for this crystal area additional light loss at the crystal edges due to the SiPM wire bonds prohibiting a 1:1 coupling could have been the main reason for the observed CTR deterioration and, therefore, further tests will not consider this crystal cross-section anymore. On the other hand the CTR performance is similar with a crystal cross-section of $1 \times 1\,\mathrm{mm}^2$ and $2 \times 2\,\mathrm{mm}^2$, for 3mm and 20mm long crystals, as can be seen on the right hand side of figures 9 and 10. Larger CTR fluctuations for the $1 \times 1\,\mathrm{mm}^2$ cross-section measurements are caused by a lower measurement statistics due to a smaller solid angle of 511keV gamma collection.

A summary of the measured CTR with different crystal cross-sections for various lengths can be seen in table 2 and 3, measured at 12.5V overvoltage and optimum threshold. We consistently observe a CTR deterioration of around 7ps FWHM if the crystal cross-section increases from

2016 JINST 11 P08008

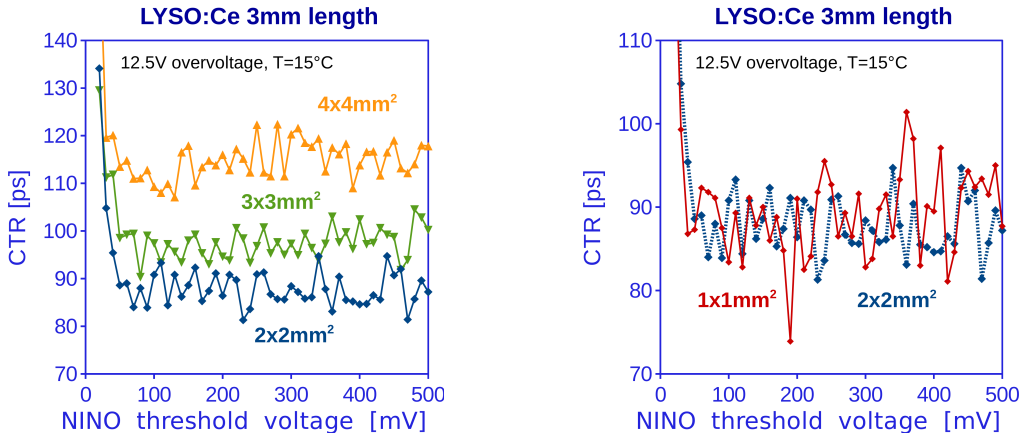

(a) (b)

Figure 9. (a) CTR versus NINO threshold voltage of the NUV-HD coupled to 3mm long LYSO:Ce scintillators with $2 \times 2\,\mathrm{mm}^2$ cross-section leads to a value of 87±3ps FWHM, $3 \times 3\,\mathrm{mm}^2$ to 95±2ps FWHM and $4 \times 4\,\mathrm{mm}^2$ to 111±2ps FWHM. (b) Direct comparison of $2 \times 2 \times 3\,\mathrm{mm}^3$ LYSO:Ce (already shown in subplot a) and $1 \times 1 \times 3\,\mathrm{mm}^3$ LYSO:Ce shows no significant CTR difference. Note: each CTR "point" in the shown figures represents an individual, newly performed, measurement. Hence, the seen fluctuations in the CTR are directly linked to their statistical measurement errors.

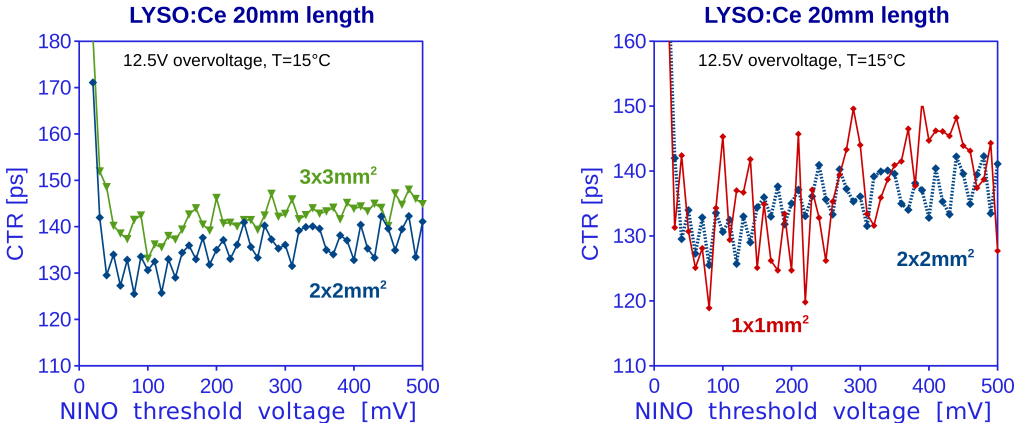

(a) (b)

Figure 10. (a) CTR versus NINO threshold voltage of the NUV-HD coupled to 20mm long LYSO:Ce scintillators with $2 \times 2\,\mathrm{mm}^2$ cross-section leads to a value of 130±3ps FWHM and $3 \times 3\,\mathrm{mm}^2$ to 137±3ps FWHM. (b) Direct comparison of $2 \times 2 \times 20\,\mathrm{mm}^3$ LYSO:Ce (already shown in subplot a) and $1 \times 1 \times 20\,\mathrm{mm}^3$ LYSO:Ce shows no significant CTR difference. Note: each CTR "point" in the shown figures represents an individual, newly performed, measurement.

$2 \times 2\,\mathrm{mm}^2$ to $3 \times 3\,\mathrm{mm}^2$ for 3mm, 5mm and 20mm long LYSO:Ce crystals (as can be seen in table 2 and in figures 9 and 10). Table 3 confirms this observation for LSO:Ce codoped with 0.2%Ca crystals from the producer Agile. For LSO:Ce:0.2%Ca it is worth to notice that the best CTR measured for $2 \times 2 \times 20\,\mathrm{mm}^3$ crystals is 117±3ps FWHM. A slightly better value compared to LSO:Ce:0.4%Ca of 122±3ps FWHM, which could be explained by a smaller light absorption in LSO:Ce:0.2%Ca crystals, as can be seen on the right hand side of figure 4. This assumption

2016 JINST 11 P08008

Table 2. Summary of CTR values measured for different crystal cross-sections and lengths with LYSO:Ce. Values are evaluated on grounds of the CTR versus threshold scans, for which six points in the vicinity of the minimum were averaged. This leads to a lower statistical fluctuation (measurement error), as every CTR point in the threshold scans represents an individual (statistically independent) measurement.

LYSO:Ce (CPI) crystal cross-section [mm^2]	CTR [ps] 3mm length	CTR [ps] 5mm length	CTR [ps] 20mm length
1×1	87±3		130±5
2×2	87±3	95±2	130±3
3×3	95±2	104±2	137±3
4×4	111±2		

Table 3. Summary of CTR values measured for different crystal cross-sections and lengths with LSO:Ce codoped with 0.2%Ca. Values are evaluated on grounds of the CTR versus threshold scans, for which six points in the vicinity of the minimum were averaged.

LSO:Ce:0.2%Ca (Agile) crystal cross-section [mm^2]	CTR [ps] 3mm length	CTR [ps] 20mm length
2×2	75±3	117±3
3×3	82±2	126±2

is supported by relative light output measurements with a R2059 PMT (normalized to LYSO:Ce) giving 84% for LSO:Ce:0.2%Ca and 67% for LSO:Ce:0.4%Ca with $2 \times 2 \times 20\,\text{mm}^3$ size, wrapped in Teflon and coupled with Rhodorsil 47V.

If we investigate the CTR deterioration with increasing crystal cross-section as a function of SiPM bias voltage, as can be seen in figure 11, we observe that the relative time resolution deterioration worsens with increasing bias voltage. This could be a hint that the increasing gain and, hence, the increasing optical crosstalk probability in the SiPM could explain at least part of the observed CTR deterioration.

3.4 Time resolution with GAGG:Ce and codoped with Mg

Apart from TOF-PET, the natural radioactivity of Lutetium could be a problem in some applications where timing is crucial. For this reason, newly developed GAGG:Ce crystals codoped with Mg can be a valid option to replace Lutetium based scintillators [5]. In order to study the potential of this crystal in terms of timing we measured the CTR of GAGG:Ce and GAGG:Ce codoped with Mg coupled to NUV-HD SiPMs, as can be seen in figure 12.

The best CTR value achieved with GAGG:Ce is 480±45ps FWHM, whereas we achieve a CTR of 200±18ps FWHM with the same crystal compound if codoped with Mg. This improvement in time resolution can be explained by a much faster scintillation rise time and faster scintillation decay time with codoped Mg crystals, as can be seen in table 1 and in [5]. The crystal dimensions where $2 \times 2 \times 10\,\text{mm}^3$ wrapped in Teflon and coupled to the SiPM with Meltmount ($n = 1.68$). For comparison we as well show in figure 12 the obtained best CTR of 100±3ps FWHM with LSO:Ce codoped 0.4%Ca crystals of the same dimensions. With standard LYSO:Ce crystals from

2016 JINST 11 P08008

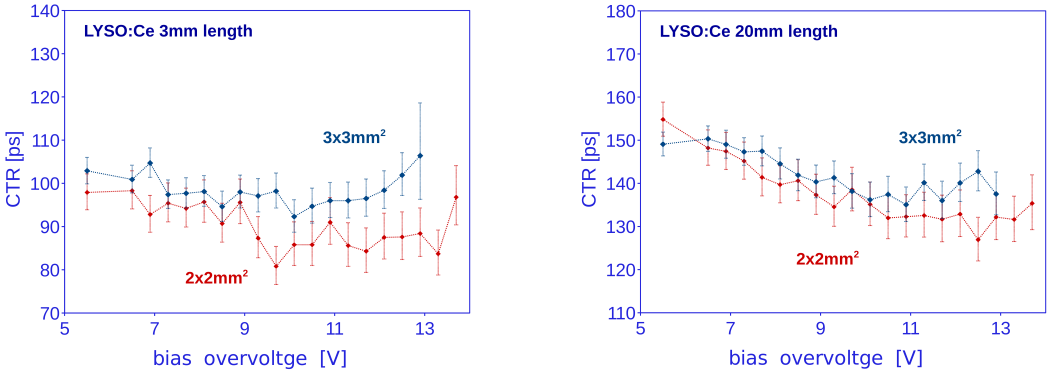

(a) (b)

Figure 11. The CTR as a function of SiPM bias overvoltage shows that at higher overvoltages the CTR deteriorates more with increasing crystal cross-section, which could be a hint of an increased optical crosstalk with increased bias overvoltage playing a role. (a) for $2\times2\times3$ mm^3 and $3\times3\times3$ mm^3; (b) for $2\times2\times20$ mm^3 and $3\times3\times20$ mm^3 LYSO:Ce crystals from CPI.

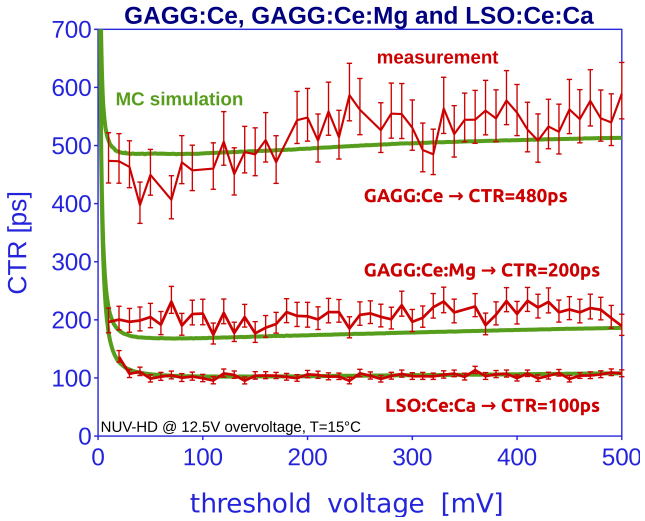

Figure 12. CTR measurements with the NUV-HD and $2\times2\times10$ mm^3 GAGG:Ce and GAGG:Ce codoped with Mg crystals result in best values of 480±45ps FWHM and 200±18ps FWHM, respectively. The CTR of LSO:Ce codoped 0.4%Ca leading to a value of 100±3ps is shown for comparison. Green solid lines represent the outcome of Monte Carlo simulations taking into account the measured scintillation rates and light yields of the crystals [5].

CPI and the same dimensions we measured a CTR of 113±3ps FWHM (as can be seen in figure 7). We further are able to estimate the measured CTR with comprehensive Monte-Carlo simulations (described in [2]), taking into account the independently measured scintillation properties, as shown in table 1, which is represented by the green solid lines in figure 12.

3.5 Time resolution with LuAG:Pr, LuAG:Ce and codoped with Ca

Recently it was shown that the scintillation properties of LuAG:Ce crystals can be improved substantially by codoping with divalent ions such as Mg^{2+} and Ca^{2+} [4, 6, 7]. Because of the faster

2016 JINST 11 P08008

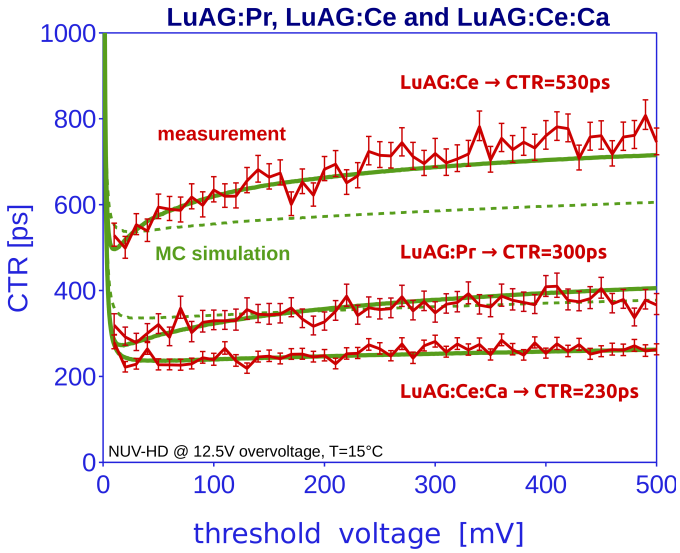

Figure 13. CTR measurements with the NUV-HD and $2 \times 2 \times 8\,\mathrm{mm}^3$ LuAG:Ce and LuAG:Ce codoped with Ca crystals result in a best value of 530±28ps FWHM and 230±15ps FWHM, respectively. The best achievable CTR value for LuAG:Pr is 300±20ps FWHM, despite the used Meltmount glue with its cut-off wavelength of ~400nm. Green solid lines represent the outcome of Monte Carlo simulations taking into account the measured scintillation rates and light yields of the crystals including Cherenkov photons. The green dotted lines show Monte Carlo simulations assuming that no Cherenkov photons are being detected.

scintillation rise- and decay times observed in LuAG:Ce codoped with Ca together with a large suppression of long tailed decay-components the CTR measurements with LuAG:Ce:Ca yield much better results as compared to LuAG:Ce, as can be seen in figure 13.

For LuAG:Ce we measured a CTR of 530±28ps which improves to 230±15ps FWHM if codoped with Calcium, measurements were performed with $2 \times 2 \times 8\,\mathrm{mm}^3$ sized crystals. Standard LuAG:Pr achieves a CTR of 300±20ps FWHM, however, it should be mentioned that the chosen Meltmount coupling with its cut-off at around 400nm is not beneficial for the LuAG:Pr emission in the near ultraviolet. In figure 13 the green solid lines represent comprehensive Monte Carlo simulations (as described in our former publication [2]), which are able to estimate the CTR as a function of the threshold voltage. We want to point out that in order to simulate correctly it is important to include Cherenkov photons in the Monte Carlo simulations, i.e. 3.4 photoelectrons detected for LuAG:Pr and 1.7 photoelectrons detected for LuAG:Ce [7]. In figure 13 the solid green lines represent the MC simulations including the estimated Cherenkov photon yields, whereas the dotted green lines show simulations with the number of Cherenkov photons set to zero. From this test we indeed infer that the inclusion of prompt photons (Cherenkov) produced in the scintillator is important to fully understand the CTR as a function of the leading edge discrimination threshold.

4 Discussion

4.1 Scintillator light output with different cross-sections

One reason for the observed worsening of the CTR with increasing crystal cross-section could be a changed light output of the crystals. In order to test this we measured the light output of our samples

2016 JINST 11 P08008

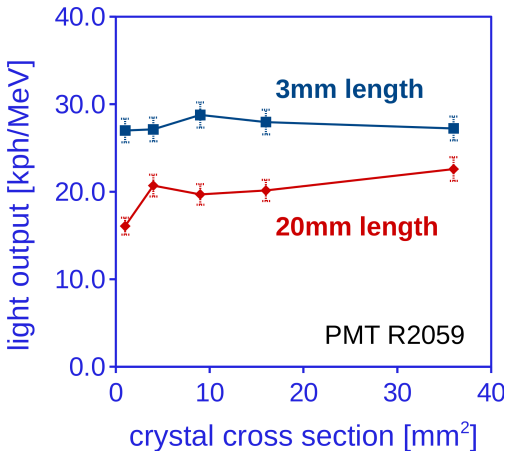

Figure 14. Light output of 3mm and 20mm long LYSO:Ce crystals versus the crystal cross-section (1×1, 2×2, 3×3, 4×4 and $6 \times 6\,\mathrm{mm}^2$). No significant difference in light output is seen with different crystal cross-sections. Measurements were performed with a Hamamatsu R2059 PMT and values are corrected for the quantum efficiency of the PMT.

versus the crystal cross-section for 3mm and 20mm long crystals, as can be seen in figure 14. The crystals were wrapped in Teflon (minimum 5 layers) and coupled to the used PMT R2059 with Rhodorsil 47V ($n = 1.42$) grease.

No significant difference in light output is observed apart from the $1 \times 1 \times 20\,\mathrm{mm}^3$ crystals, which show a slightly lower value. The difference in light output for $1 \times 1 \times 20\,\mathrm{mm}^3$ crystals can be explained by the higher amount of diffusive reflections (edge diffusion) due to the larger aspect ratio, resulting in a higher absorption or loss [16]. Nevertheless, it should be noted that light emitted in a small angle directly towards the photodetector is undergoing total internal reflection on the side walls and therefore being transfered rather efficiently, despite multiple reflections. This light, in fact, determines the CTR largely and therefore smaller cross-section crystals perform very similar in timing as compared to crystals with larger cross-sections, as can be seen in figures 9 and 10.

4.2 Single photon time resolution

The single photon time resolution (SPTR) of the NUV-HD SiPM was measured with a 420nm PiLas picosecond laser from the producer Advanced Laser Diode Systems A.L.S. GmbH. The light intensity was reduced with optical filters to the extent that the photons detected by the SiPM were at the level of a single photon for each pulse. In addition we selected in the offline data analysis only events corresponding to single photoelectrons. This was done by splitting and recording the SiPM amplitude separately from the NINO signal, similar to the CTR measurements discussed in section 2.2. The used PiLas laser has a pulse width of around 42ps FWHM, which is small enough to be negligible for the ensuing SPTR measurements. In figure 15 we show the SPTR in FWHM measured with the NUV-HD SiPM ($4 \times 4\,\mathrm{mm}^2$ and $25\,\mu$m SPAD size).

We investigated different areas of illumination, i.e. the whole SiPM illuminated uniformly by the incoming picosecond pulsed laser light ("No Mask"), a "2mm Mask" only illuminating an area of $2 \times 2\,\mathrm{mm}^2$ centered in the middle of the SiPM, a "500μm Mask" illuminating a $0.5 \times 0.5\mathrm{mm}^2$ area and the laser beam being focused in the center of a single SPAD with a spot size smaller 10μm

2016 JINST 11 P08008

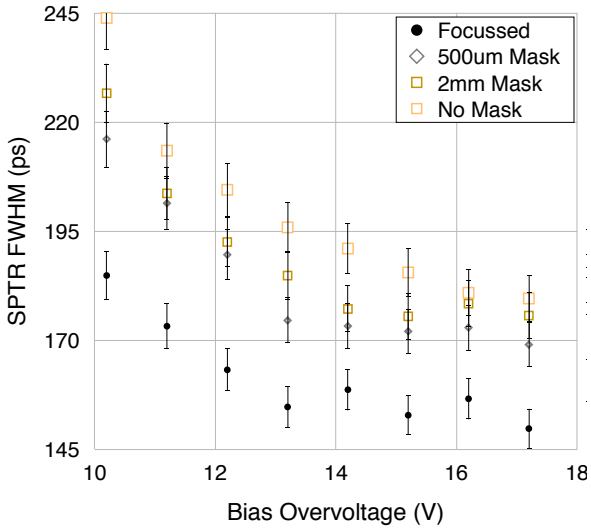

Figure 15. Single photon time resolution of the NUV-HD with $4 \times 4\,\mathrm{mm}^2$ device and $25 \times 25\,\mu\mathrm{m}^2$ SPAD size. The SPTR only changes marginally if the light illumination is restricted to areas smaller than the SiPM size. Focussing the light in the center of one SPAD, however, improves the SPTR significantly due to border effects in the SPAD being eliminated.

("Focussed"). There is only a small SPTR difference observed for the SiPM being illuminated with different mask sizes, having slightly better values if the illuminated area is getting smaller. This is explained by a decreased signal transfer time spread of the electrical signals for smaller areas [20]. However, the NUV-HD SiPM is already optimized to reduce this effect largely. If the laser light is focussed within one SPAD we observe a significant improvement in the SPTR value to 150ps FWHM. We could explain this improvement by "border effects" in the SPAD worsening the SPTR, which are not observed if the laser spot is focussed in the middle of one SPAD.

It is important to mention that the measured SPTR of 180ps FWHM (illuminating a $2 \times 2\,\mathrm{mm}^2$ area) is influenced by electronic noise [21]. We estimated the electronic noise influence to the SPTR with measurements similar to the method described in section 3.2. Deconvolving the measured electronic noise contribution, the "real" SiPM SPTR is lower and around 115ps FWHM.

As already mentioned, there is only a slight change in the SPTR with different mask sizes (at maximum 20ps FWHM for 13V overvoltage), as shown in figure 15. A worse SPTR for larger active SiPM areas is indeed an important factor in order to explain the observed CTR deterioration with increasing crystal cross-section. However, from Monte Carlo simulations (described in [2]) we estimated that the measured change in SPTR can only account partially for the measured CTR deterioration. This can be seen in figure 16, which shows simulations of the CTR for LSO:Ce:0.2%Ca with $2 \times 2 \times 3\,\mathrm{mm}^3$ size as a function of the SPTR in FWHM. The MC data can be fitted with $\sqrt{SPTR^{1.556} + 63^2}$, shown as red solid line in figure 16. With this fit-function we can evaluate that a SPTR change of 20ps FWHM (as can be deduced from figure 15) leads to a CTR change of only 3ps and, hence, can only account to maximum half the measured CTR deterioration with increasing crystal cross-section. This can be understood by the photon travel spread in the crystal, which has a similar magnitude as the SPTR [18], leading to a smaller sensitivity of SPTR

2016 JINST 11 P08008

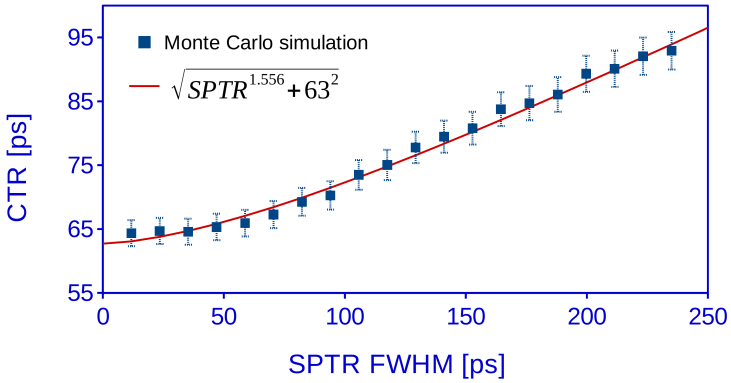

Figure 16. Monte Carlo simulations show that the measured change in SPTR for different illuminated SiPM areas has only a slight influence on the CTR. A change in SPTR of 20ps FWHM only leads to a change in CTR of 3ps FWHM.

changes on the CTR. Additionally, electronic noise (discussed in section 3.2) leads to a worse CTR if the leading edge threshold for best timing is low, as in the case of a low SPTR [2].

4.3 Baseline shift influence

Another possible reason for a deterioration of the CTR with a larger crystal cross-section could be an increased noise floor (either due to dark counts or a larger crosstalk probability) and, hence, amplified baseline shifts. In order to estimate the baseline-shift influence on the CTR we measured the timing with different filters coupling the SiPM signal to NINO. On the left hand side of figure 17 it can be seen that different high-pass filters (100pF and 10pF) do not significantly change the best achieved CTR, where the crystal size is $3\times3\times3\,\mathrm{mm}^3$. Even a more rigorous pole-zero compensation technique [22] does not improve the CTR, as can be seen on the right hand side of figure 17. Similar results were obtained for longer crystals, i.e. $3\times3\times20\,\mathrm{mm}^3$, as can be seen in figure 18. From these measurements we are confident that baseline-shifts do not influence the CTR significantly, at least for the given NUV-HD SiPM and electronics.

4.4 Increased optical crosstalk probability due to a coupled scintillator

In figures 9 and 10 we have measured a ~7ps FWHM deterioration in CTR with increasing crystal cross-section ($2\times2\,\mathrm{mm}^2$ to $3\times3\,\mathrm{mm}^2$). This deterioration was confirmed with different crystal types and renewed coupling and wrapping, allowing us to exclude a systematic bias from these effects. We showed that the light output of the crystal and baseline-fluctuations are not the reason for the observed CTR degradation. Furthermore, we have partly excluded an increase of the SPAD signal transfer time spread and thus SPTR with increased illuminated area of the SiPM being the whole reason for the seen CTR deterioration, because it could not account for the complete amount seen. Another possibility to explain the CTR deterioration with increasing crystal cross-section could be an increase in optical crosstalk probability caused by the scintillator acting as a reflector [11].

Figure 19 shows staircase plots for 12.5V overvoltage measured with various configurations; no crystal coupled to the SiPM or with coupled 3mm or 20mm long crystals and different cross-sections, i.e. $1\times1\,\mathrm{mm}^2$, $2\times2\,\mathrm{mm}^2$ and $3\times3\,\mathrm{mm}^2$. It can be seen that the crosstalk probability

2016 JINST 11 P08008

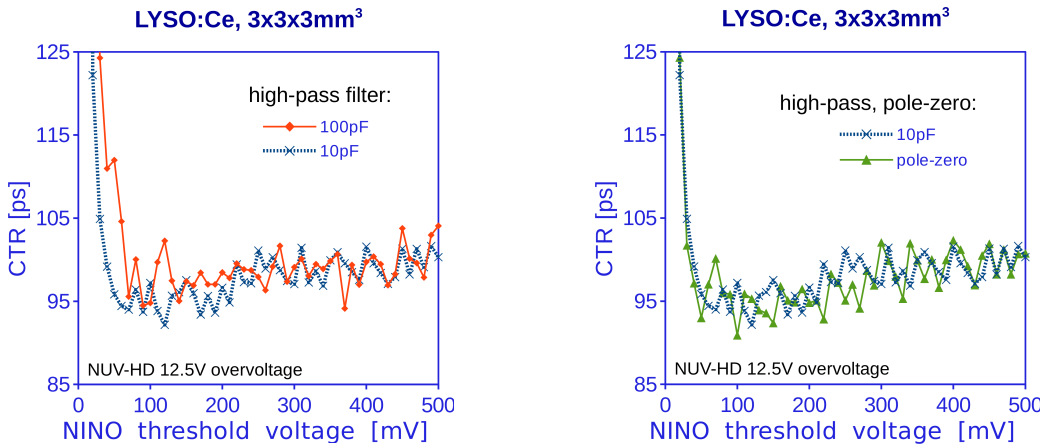

(a) (b)

Figure 17. Baseline shift corrections with (a) different high pass filters (100pF and 10pF) or (b) a more refined pole-zero compensation do not show significant differences in the CTR. Measured with $3\times3\times3$ mm^3 LYSO:Ce scintillators coupled to NUV-HD at an overvoltage of 12.5V and 15°C.

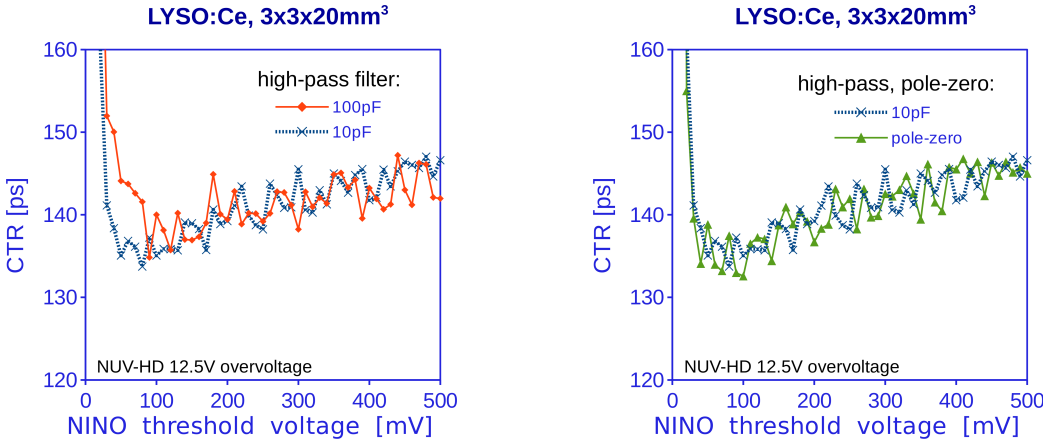

(a) (b)

Figure 18. Baseline shift corrections with (a) different high pass filters (100pF and 10pF) or (b) a more refined pole-zero compensation do not show significant differences in the CTR. Measured with $3\times3\times20$ mm^3 LYSO:Ce scintillators coupled to NUV-HD at an overvoltage of 12.5V and 15°C.

rises with increasing crystal cross-section, as the crystal acts as a reflector for the generated optical photons in the SiPM within an avalanche. In figure 20 similar measurements are shown, now performed with an overvoltage of 6.5V. Reducing the overvoltage from 12.5V to 6.5V the crosstalk probability reduces, mainly because of a lower gain.

Besides the increase in baseline fluctuations, which we excluded to be the reason for the CTR degradation, this increase in crosstalk induces as well an excess noise factor in the scintillation statistics and thus leads to a worsening of the CTR [23]. In order to qualitatively investigate this influence we performed Monte Carlo simulations as described in [2]. In these simulations we set the i^{th} crosstalk probability to $P_i = \exp(-i/\tau_{\text{XT}})$, where τ_{XT} can be seen as a crosstalk "decay" parameter, i.e. the smaller τ_{XT} the smaller the crosstalk probability and less consecutive (additive)

2016 JINST 11 P08008

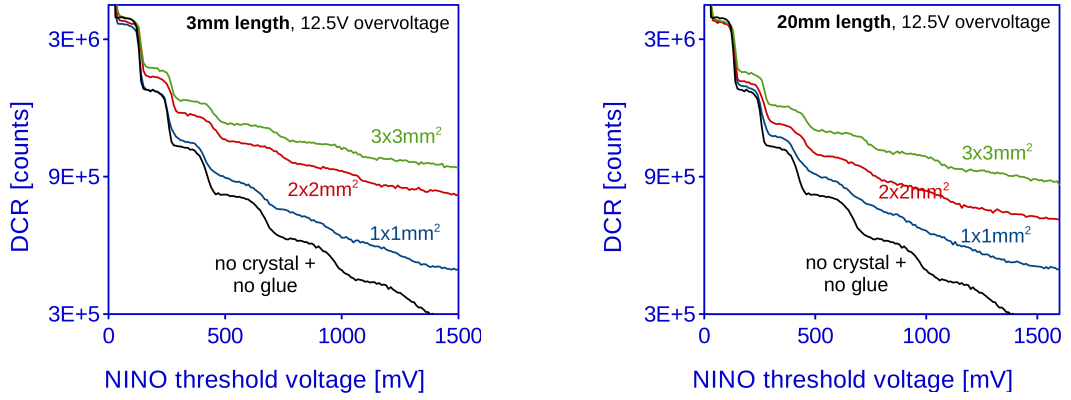

(a) (b)

Figure 19. Staircase plots for (a) 3mm and (b) 20mm long crystals measured at a SiPM overvoltage of 12.5V. Measurements were performed with four different configurations: sole SiPM with cleaned surface and crystals mounted to the SiPM with three different cross-sections, i.e. 1×1 mm^2, 2×2 mm^2 and 3×3 mm^2.

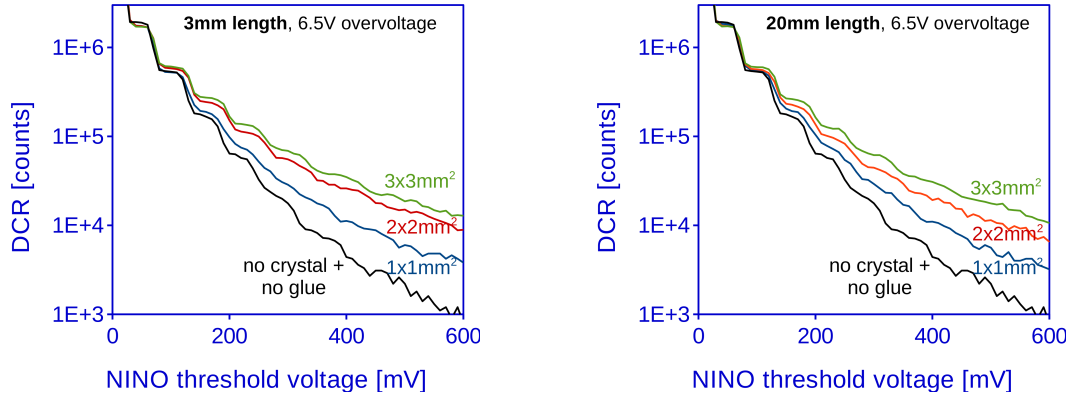

(a) (b)

Figure 20. Staircase plots for (a) 3mm and (b) 20mm long crystals measured at a SiPM overvoltage of 6.5V. Measurements were performed with four different configurations: sole SiPM with cleaned surface and crystals mounted to the SiPM with three different cross-sections, i.e. 1×1 mm^2, 2×2 mm^2 and 3×3 mm^2.

events. If the parameter i equals zero ($i = 0$), the probability P_i is one ($P_i = 1$), which in this case represents the normal photon detection. We suppose that each crosstalk event has an increased time smearing ($\sigma = SPTR \cdot \sqrt{i+1}$) and an additional time delay ($\mu = \mu_0 + SPTR \cdot \sqrt{i}$) with μ_0 being the time delay of the detected photoelectron ($i = 0$). The outcome of this simulation study can be seen in figure 21. One can see that for high crosstalk probabilities in the order of $> 65\%$ ($1/\tau_{XT} < 0.44$) the CTR starts to deteriorate. This is consistent with the crosstalk probabilities deduced from the staircase plots shown in figure 19, as we can fit the parameter $1/\tau_{XT}$ to 0.53 for 1×1 mm^2, 0.44 for 2×2 mm^2 and 0.34 for 3×3 mm^2 crystal cross section and 12.5V overvoltage.

The lower observed crosstalk probability for lower bias overvoltages would in this simple model lead to no observable CTR deterioration. This is confirmed by the lower CTR deterioration with increasing crystal cross-section observed for lower SiPM bias overvoltages as compared to higher bias overvoltages, which can be seen in figure 11. In this model the remaining CTR deterioration

2016 JINST 11 P08008

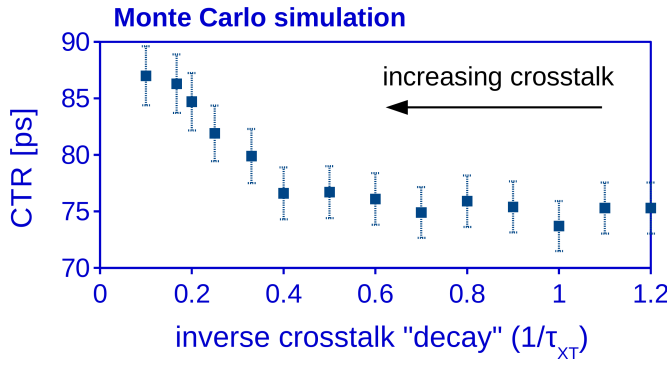

Figure 21. Monte Carlo simulations on how an increased crosstalk probability could influence the CTR. Only for very high crosstalk probabilities a CTR deterioration in the order of 10ps FWHM is observed.

with higher crystal cross-sections at lower bias overvoltages could be explained by an increased SPTR due to an increased signal transfer time spread with a larger active SiPM area, as was discussed in section 4.2. We want to mention that the simple toy-model described above certainly does not represent the real time structure of crosstalk events, which by definition are not independently distributed. Simply because the n^{th} crosstalk event depends on the $(n-1)^{\text{th}}$ event. This simple model should merely show that there can be a possible influence of direct crosstalk events to the CTR, if the crosstalk probability is high enough. In summary, we have to conclude that a precise measurement and modeling (including the crystal) of the time structure of crosstalk events for various overvoltages has to be anticipated in future, in order to give a more precise insight on how crosstalk events could deteriorate the CTR in analog-SiPM based TOF-PET systems.

5 Conclusions

We have shown that the newest SiPM technology from FBK, i.e. the NUV-HD, can achieve a coincidence time resolution of 73±2ps FWHM if coupled to $2 \times 2 \times 3\,\text{mm}^3$ LSO:Ce codoped 0.4%Ca crystals. In PET a high 511keV detection efficiency is important, which calls for the need of longer crystals. In this respect LSO:Ce codoped 0.2%Ca crystals with a size of $2 \times 2 \times 20\,\text{mm}^3$ are able to achieve a best CTR of 117±3ps FWHM. Using more standard LYSO:Ce this value would be 130±3ps FWHM for similar scintillator sizes. Increasing the crystal cross-section leads to a deterioration in the CTR which we attributed partly to an increased single photon time resolution of the SiPM due to an increased signal transfer time spread seen with larger active SiPM areas. Another factor deteriorating the CTR for larger crystal cross-sections might be an increased optical crosstalk due to the crystal itself acting as a reflector for optical photons generated in the avalanche. However, further studies in this direction are necessary (e.g. with $6 \times 6\,\text{mm}^2$ sized SiPMs) to fully conclude on the exact size of these different contributions. Finally, we tested GAGG:Ce and LuAG:Ce and confirmed that codoping with Magnesium or Calcium can improve significantly the scintillation properties and therefore the achievable time resolution.

Acknowledgments

This work has been performed in the context of the TICAL project, ERC Advanced Grant (PI P. Lecoq) #38953, Grant Agreement 289355-PicoSEC-MCNet, the Crystal Clear Collaboration and

2016 JINST 11 P08008

COST Action TD1401 (FAST). Devices were developed with the support of the European Community Seventh Framework Programme (EU FP7) Project SUB nanosecond Leverage In PET/MR ImAging (SUBLIMA) under Grant #241711. Further we want to thank A. Petrosyan for providing the LuAG:Ce(:Ca) samples and M. Nikl for providing the GAGG:Ce(:Mg) samples used in this study.

References

[1] S. Seifert et al., *A comprehensive model to predict the timing resolution of SiPM-based scintillation detectors: theory and experimental validation*, *IEEE Trans. Nucl. Sci.* **59** (2012) 190.

[2] S. Gundacker et al., *Time of flight positron emission tomography towards 100ps resolution with L(Y)SO: an experimental and theoretical analysis*, 2013 *JINST* **8** P07014.

[3] C. Piemonte et al., *Performance of NUV-HD silicon photomultiplier technology*, *IEEE Trans. Electron. Dev.* **63** (2016) 1111.

[4] A. Petrosyan et al., *A study of radiation effects on LuAG:Ce(Pr) co-activated with Ca*, *J. Cryst. Growth* (2015) 46.

[5] M. Lucchini et al., *Effect of Mg^2+ ions co-doping on timing performance and radiation tolerance of Cerium doped $Gd_3Al_2Ga_3O_{12}$ crystals*, *Nucl. Instrum. Meth.* **A 816** (2016) 176.

[6] M. Nikl et al., *Defect engineering in Ce-dopded aluminum garnet single crystals scintillators*, *Cryst. Growth Design* **14** (2014) 4827.

[7] S. Gundacker et al., *Measurement of intrinsic rise times for various L(Y)SO and LuAG scintillators with a general study of prompt photons to achieve* 10 *ps in TOF-PET*, *Phys. Med. Biol.* **61** (2016) 2802.

[8] S. Omelkov et al. *New features of hot intraband luminescence for fast timing*, *J. Luminesc.* **176** (2016) 309.

[9] S.E. Brunner et al., *Studies on the Cherenkov effect for improved time resolution of TOF-PET*, *IEEE Trans. Nucl. Sci.* **61** (2014) 443.

[10] S. Korpar et al., *Study of TOF PET using Cherenkov light*, *Nucl. Instrum. Meth.* **A 654** (2011) 532.

[11] A. Gola et al., *SiPM optical crosstalk amplification due to scintillator crystal: effects on timing performance*, *Phys. Med. Biol.* **59** (2014) 3615.

[12] M.V. Nemallapudi et al., *Sub-*100 *ps coincidence time resolution for positron emission tomography with LSO:Ce codoped with Ca*, *Phys. Med. Biol.* **60** (2015) 4635.

[13] F. Anghinolfi et al., *NINO: an ultrafast low-power front-end amplifier discriminator for the time-of-flight detector in the ALICE experiment*, *IEEE Trans. Nucl. Sci.* **51** (2004) 1974.

[14] S. Gundacker, *Time resolution in scintillator based detectors for positron emission tomography*, Ph.D. thesis, Vienna University of Technology, Vienna, Austria (2014).

[15] R. Turtos et al., *Measurement of LYSO intrinsic light yield using electron excitation*, *IEEE Trans. Nucl. Sci* **63** (2016) 475.

[16] K. Pauwels et al., *Effect of aspect ratio on the light output of scintillators*, *IEEE Trans. Nucl. Sci.* **59** (2012) 2340.

[17] S. Gundacker et al., *On the comparison of analog and digital SiPM readout in terms of expected timing performance*, *Nucl. Instrum. Meth.* **A 787** (2015) 6.

2016 JINST 11 P08008

[18] S. Gundacker et al., *Time resolution deterioration with increasing crystal length in a TOF-PET system*, *Nucl. Instrum. Meth.* **A 737** (2014) 92.

[19] S. Surti et al., *Performance of philips gemini TF PET/CT scanner with special consideration for its time-of-flight imaging capabilities*, *J. Nucl. Med.* **48** (2007) 471.

[20] F. Acerbi et al., *Analyisis of transit time spread on FBK silicon photomultipliers*, 2015 *JINST* **10** P07014.

[21] F. Acerbi et al., *Characterization of single-photon time resolution: from single SPAD to silicon photomultiplier*, *IEEE Trans. Nucl. Sci.* **61** (2014) 2678.

[22] A. Gola et al., *Analog circuit for timing measurements with large area SiPMs coupled to LYSO crystals*, *IEEE Trans. Nucl. Sci* **60** (2013) 1296.

[23] S. Vinogradov, *Analytical model of SiPM time resolution and order statistics with crosstalk*, *Nucl. Instrum. Meth.* **A 787** (2015) 229.

2016 JINST 11 P08008